Published in final edited form as:

Biochim Biophys Acta Mol Cell Biol Lipids. 2020 April ; 1865(4): 158609. doi:10.1016/j.bbalip.2020.158609.

Stable reduction of STARD4 alters cholesterol regulation and lipid homeostasis

David B. Iaea[1,2,#], **Zachary R. Spahr**[1,#], **Rajesh K. Singh**[1,#], **Robin B. Chan**[3], **Bowen Zhou**[3], **Rohan Bareja**[4], **Olivier Elemento**[4], **Gilbert Di Paolo**[3,5], **Xiaoxue Zhang**[1], **Frederick R. Maxfield**[1,2]

[1]Department of Biochemistry, Weill Cornell Medical College, 1300 York Ave, New York, NY, 10065, USA.

[2]Weill Cornell Medical College, Rockefeller University, and Memorial Sloan-Kettering Cancer Center Tri-Institutional Chemical Biology Program, New York, NY 10065, USA.

[3]Pathology and Cell Biology, Taub Institute for Research on Alzheimer's Disease and the Aging Brain, Columbia University Medical Center, New York, NY 10032, USA.

[4]Institute for Computational Biomedicine, Department of Physiology and Biophysics, Weill Cornell Medical College, 1300 York Ave, New York, NY, 10065, USA.

Abstract

STARD4, a member of the evolutionarily conserved START gene family, is a soluble sterol transport protein implicated in cholesterol sensing and maintenance of cellular homeostasis. STARD4 is widely expressed and has been shown to transfer sterol between liposomes as well as organelles in cells. However, STARD4 knockout mice lack an obvious phenotype, so the overall role of STARD4 is unclear. To model long term depletion of STARD4 in cells, we use short hairpin RNA technology to stably decrease STARD4 expression in human U2OS osteosarcoma cells (STARD4-KD). We show that STARD4-KD cells display increased total cholesterol , slower cholesterol trafficking between the plasma membrane and the endocytic recycling compartment, and increased plasma membrane fluidity. These effects could all rescued by transient expression of a short hairpin RNA-resistant STARD4 construct. Some of the cholesterol increase was due to excess storage in late endosomes or lysosomes. To understand the effects of reduced STARD4, we carried out transcriptional and lipidomic profiling of control and STARD4-KD cells. Reduction of STARD4 activates compensatory mechanisms that alter membrane composition and lipid homeostasis. Based on these observations, we propose that STARD4 functions as a critical sterol transport protein involved in sterol sensing and maintaining lipid homeostasis.

Keywords

Cholesterol; lipids; lipidomics; computational biology; membrane lipids; gene expression

Corresponding Author: Frederick R. Maxfield, Department of Biochemistry, Box 63, Weill Cornell Medical College, 1300 York Avenue, New York, NY 10065, frmaxfie@med.cornell.edu, Tel: 212 746 6405, Fax: 212 746 8875.

[5]Present address: Denali Therapeutics Inc., 201 Gateway Blvd, South San Francisco, CA 94080

[#]These authors contributed equally to this work.

INTRODUCTION:

Significant differences in sterol concentration are maintained among cellular organelles. In the plasma membrane of mammalian cells cholesterol is 35 mol% or more of the total lipids [1-3], but cholesterol accounts for only about 5 mol% of lipids in the endoplasmic reticulum (ER) [4-8]. The cholesterol-phospholipid ratio in the Golgi is intermediate between the plasma membrane and the ER [7]. In several cell types, the endocytic recycling compartment (ERC) has been shown to be a major pool of intracellular cholesterol [9-13]. The heterogeneous distribution of cholesterol among cellular membrane compartments can be attributed, in part, to the differences in the organelle lipid composition [1, 2, 14].

Cellular cholesterol levels are tightly regulated by coordinated homeostatic mechanisms, primarily involving the regulated proteolysis of the sterol responsive element-binding protein 2 (SREBP-2) transcription factor upon transport from the ER to the Golgi [15].

Cholesterol can move between membranes by vesicular and non-vesicular transport mechanisms [6, 12], and there is substantial evidence for high rates of non-vesicular sterol transport in cells [3, 10, 16]. Sterol transfer proteins interact with organelles to extract sterol and then deliver it to acceptor membranes [17]. There are several protein families that are classified as sterol transfer proteins, which have been shown to be capable of transferring sterols between membranes [10, 17-22]. One gene family of lipid transfer proteins that have been implicated in such trafficking is the steroidogenic acute regulatory protein (StAR)-related lipid-transfer (START) domain family [23].

There are 15 members of the mammalian START family [24] that are divided into six subfamilies based on ligand specificity and domain architecture [23, 25]. Among the cholesterol-specific and soluble START proteins, STARD4 is a highly efficient sterol transport protein [10, 11, 17, 26] that is transcriptionally regulated by SREBP-2 [27]. For these reasons, STARD4 has been implicated as an important sterol transport protein involved in maintaining cholesterol homeostasis [10, 11, 17, 25]. However, studies in mice have shown that knockout of STARD4 does not greatly alter serum cholesterol homeostasis, but it does lead to changes in gene expression of some intracellular cholesterol transporters, potentially masking a role for STARD4 [28]. Therefore, the exact functional importance of STARD4 remains unclear [10, 11, 28].

The present study examines the functional role of STARD4 in maintaining cholesterol distribution and homeostasis in cells stably depleted of STARD4. To this end, STARD4 levels were stably reduced in cells (STARD4-KD cells) using shRNA technology and rescued using shRNA-resistant STARD4 constructs. Stable reduction of STARD4 increased sterol levels. STARD4 depletion decreased the rate of sterol transport from the plasma membrane to the ERC. STARD4 reduction also increased cold Triton X-100 solubilization of the plasma membrane and increased plasma membrane fluidity. All of these effects could be rescued by expression of shRNA-resistant STARD4 constructs. We observed that some of the cholesterol in STARD4-KD cells was in organelles that contained recently internalized LDL (i.e., late endosomes or lysosomes). Changes observed in STARD4-KD cells were associated with large overall changes in lipid composition and in the expression of genes

encoding proteins involved in lipid metabolism. Among the genes affected, expression of *NPC1* and *NPC2* was reduced, and expression of STARD5 was increased. Our study provides evidence that STARD4 is a critical sterol transporter required for the maintenance of lipid homeostasis.

MATERIALS AND METHODS:

Materials

Alexa labeling kits were purchased from Invitrogen. Human transferrin (Tf) and DHE were purchased from Sigma. All tissue culture supplies were purchased from Invitrogen. All other chemicals were from Sigma. The media used are as follows: Medium 2 (150 mM NaCl, 5 mM KCl, 1 mM $CaCl_2$, 1 mM $MgCl_2$ and 20 mM HEPES, pH 7.4); M2glucose (Medium 2 containing 2 mg/ml glucose); chase medium (M2glucose containing 30ug Sandoz 58035). Low-density lipoprotein was collected via ultracentrifugation of fresh human plasma as previously described [29].

Cell culture and transfection

U2OS-SRA is a modified human osteosarcoma cell line that expresses the scavenger receptor A (SRA) [30]. U2OS-SRA cells were grown at 37° C in a 5% CO_2 humidified incubator and in McCoy's 5A medium supplemented with 10% fetal bovine serum, 1 mg/ml geneticin as a selection for SRA, 100 units/ml penicillin, and 100 ug/ml streptomycin. For stable STARD4 knockdown, U2OS-SRA cells were transfected with pGFP-V-RS shRNA encoding the target sequence 5'-GCAAGCACTTTAACCAACTTCTATGGTGA-3' (Origene) using HiPerFect transfection reagent (Qiagen) according to manufacturer's instructions. Selection of stable knockdown STARD4 U2OS-SRA cells was done with 5 μg/ml puromycin. Cells for wide-field microscopy were plated on 35-mm plastic dishes, the bottoms of which were replaced with poly-D-lysine-coated coverslips.

U2OS cells were transiently transfected with pCMV-Tag2b (Stratagene, Santa Clara, CA) plasmid containing shRNA resistant FLAG-tagged hSTARD4 or with mCherry-FKBP-hSTARD4 by electroporation using Amaxa Nucleofector II Device with the Amaxa Cell Line Nucleofector Kit V and Nucleofector Program X-001 or using FuGENE 6 transfection reagent (Promega, Madison, WI). STARD4 rescue experiments were performed 1 d after transfection.

Cell growth

U2OS-SRA and STARD4-KD cell growth was measured by plating 50,000 cells in 6 well cell culture plates and growth in U2OS media. Every 48 h cells were trypsinized and counted prior to 100% confluency.

Western blot and antibodies

Western blot experiments were performed using standard protocols. Cellular protein extracts were collected from shRNA STARD4 knockdown and control U2OS-SRA cells. Antibodies used were as follows: STARD4 (ab202060, lot number GR178227; Abcam) and Tubulin

(T9026; Sigma-Aldrich). The STARD4 antibody was validated against recombinant human STARD4.

Labeling Cells with Lipid Analogs

For DiI-C16 experiments, cells were pulsed with 10 μM dialkylindocarbocyanine DiI-C16 and shaken gently at 37°C for 30 sec, washed with M2glucose, incubated with M2glucose and either imaged immediately or pre-incubated with ice-cold M2glucose for one minute prior to incubation in ice cold 1% TX-100 for 15 minutes. Following TX-100 incubation, cells were washed three times in ice cold M2glucose and imaged immediately. Cells were labeled with dehydroergosterol (DHE) as previously described [31], with minor alterations. In brief, DHE in ethanol was dried under argon and subsequently dissolved in 25 mM methyl-β-cyclodextrin (MCD) in medium 2, making the initial ratio of MCD to DHE 5:1 (mol/mol). The resulting suspension was vortexed and sonicated until it clarified. It was then incubated in a rocking water bath overnight at 37°C and centrifuged at 15,000 × *g* for 10 min before labeling cells.

For Laurdan labeling, cells were washed with PBS and incubated with Laurdan freshly dissolved in phenol free Dulbecco modified Eagle medium (DMEM) with 2.5% FBS to a final concentration of 20 μM for 30 minutes, washed, and imaged in DMEM on a temperature controlled stage.

Fluorescent labeling and immunofluorescence

U2OS cells were stained in the dark with filipin at a final concentration of 50 ug/ml in PBS for 45 min at room temperature. Stained cells were washed three times and imaged immediately. Human transferrin (Sigma) was iron-loaded and purified by Sephacryl S-300 (Pharmacia LKB) gel-filtration chromatography and conjugated to Alexa488 or Alexa546 according to the manufacturer's instruction (Invitrogen). To label cells with Tf, cells were incubated with 20 μg/ ml Alexa546–transferrin for 20 min at 37 °C to reach steady state. LDL was conjugated to Alexa633 according to manufacturer’s instructions (Invitrogen). Cells were labeled with LDL by incubation with 10 μg/ ml LDL-Alexa633 for 1 hour at 37 °C.

Fluorescence recovery after photobleaching (FRAP)

Cells were labeled for 1 minute with DHE and chased for two hours to allow for the sterol to equilibrate among membranes. In the last twenty minutes, the cells were labeled with fluorescent transferrin to identify the ERC. A prebleach image was acquired before bleaching. DHE in the ERC was photobleached for 30 seconds, and images were taken every 30 seconds for 10 minutes. In separate experiments, cells were photobleached for 30 seconds, and six images were taken over an hour to determine the extent of recovery.

Fluorescence microscopy

Wide-field fluorescence microscopy and digital image acquisition were carried out using a Leica DMIRB microscope equipped with an Andor iXon^{EM} Blue EMCCD camera driven by MetaMorph Imaging System software (Universal Imaging/Molecular Devices, Sunnyvale, CA). All images were acquired using oil-immersion objectives 63×, 1.36 NA with 2 × 2

pixel binning. Cells being imaged were in PBS when fixed, or M2glucose when alive. DHE was imaged using a filter cube obtained from Chroma Technology (Bellows Falls, VT; 335-nm [20-nm band pass] excitation filter, 365-nm-long pass dichromatic filter, and 405-nm [40-nm band pass] emission filter). Standard TRITC and FITC cubes were obtained from Chroma. Filipin staining was imaged using an A4 filter cube (Leica, Wetzlar, Germany). Whole cell fluorescence quantification was carried out using MetaMorph image processing software (Molecular Devices, Sunnyvale, CA), as described previously [32, 33]. To quantify filipin intensity in the plasma membrane, we measured the 20th percentile pixel intensity of an individual cell and multiplied that value by the total area of that cell.

Confocal fluorescence microscopy

Cells were imaged on a Zeiss LSM 880, AxioObserver microscope equipped with a Plan-Apochromat 63× Oil 1.4 NA differential interference contrast (DIC) M27 objective in a humidified chamber at 37 °C. Laurdan was excited using 405 nm laser and emission was recorded between 440 and 470 at 5 nm steps.

Data analysis for FRAP experiments

Images of DHE FRAP experiments were analyzed using Metamorph Discovery-1 image-analysis software [10, 32]. The cell outlines were traced out manually in DHE images. The ERC was also manually outlined for each cell using the Tf-labeled images. The DHE fluorescence intensity from the outlined ERC region (F'_{ERC}) and the entire cell (F_{cell}), as well as the area of the ERC (A_{ERC}), were measured. Since DHE images were wide field images, $\mathrm{I'_{ERC}}$ not only included the fluorescence in the ERC but also included the fluorescence contributed by the regions of the plasma membrane that were directly above and below the ERC. To calculate the fluorescence contributed by the plasma membrane ($F_{\mathrm{PM\ in\ ERC}}$) in the ERC region, a small region next to the ERC was selected manually. The integrated fluorescence (F_{PM}) and the area (A_{PM}) in this region were measured.

$$F_{\mathrm{PM\ in\ ERC}} = \frac{F_{\mathrm{PM}} \times A_{\mathrm{ERC}}}{A_{\mathrm{PM}}} \qquad \text{Equation 1,}$$

was used. This was based on the assumption that the DHE fluorescence present on the plasma membrane directly above and below the ERC was similar to that on the plasma membrane next to the ERC. The DHE fluorescence only contributed from the ERC (F_{ERC}) was calculated using

$$F_{\mathrm{ERC}} = F'_{\mathrm{ERC}} - F_{\mathrm{PM\ in\ ERC}} = F'_{\mathrm{ERC}} - \frac{F_{\mathrm{PM}} \times A_{\mathrm{ERC}}}{A_{\mathrm{PM}}}. \qquad \text{Equation 2,}$$

In FRAP experiments, $F_{\mathrm{ERC}}/F_{\mathrm{cell}}$ was used to determine the fluorescence recovery ratio. FRAP data were fitted using Matlab to Equation 3, $f(t) = 1 - e^{-at}$. All data were analyzed with MetaMorph image analysis software (Molecular Devices, Downingtown, PA).

Laurdan image analysis

GP values were calculated by comparing the Laurdan intensity at 440 and 470 nm according to the GP equation.

$$GP = \frac{I_{440} - I_{470}}{I_{440} + I_{470}} \quad \text{Equation 4,}$$

Background noise (less than 2% maximum signal) was excluded and GFP signal (less than 1% maximum signal) was corrected for in STARD4 KD cells at 470 nm. Representative images were analyzed in MetaMorph image analysis software (Molecular Devices, Downingtown, PA), resulting in ratio images where color indicates GP and the summed intensity at 440 nm and 470 nm is the final image intensity.

Lipid Extraction

Lipid extracts of wild type and STARD4 knockdown U2OS-SRA cells were prepared using a modified Bligh/Dyer extraction procedure [34].

Analysis of Lipids Using High Performance Liquid Chromatography-Mass Spectrometry

Lipid extracts were prepared using modified Bligh/Dyer extraction procedure spiked with appropriate internal standards, and analyzed using a 6490 Triple Quadrupole LC/MS system (Agilent Technologies, Santa Clara, CA). Glycerophospholipids and sphingolipids were separated with normal-phase HPLC as described before [34], with a few modifications. An Agilent Zorbax Rx-Sil column (inner diameter 2.1 x 100 mm) was used under the following conditions: mobile phase A (chloroform:methanol:1 M ammonium hydroxide, 89.9:10:0.1, v/v) and mobile phase B (chloroform:methanol:water:ammonium hydroxide, 55:39.9:5:0.1, v/v); 95% A for 2 min, linear gradient to 30% A over 18 min and held for 3 min, and linear gradient to 95% A over 2 min and held for 6 min. Sterols and glycerolipids were separated with reverse-phase HPLC using an isocratic mobile phase as before [34] except with an Agilent Zorbax Eclipse XDB-C18 column (4.6 x 100 mm).

Quantification of lipid species was accomplished using multiple reaction monitoring (MRM) transitions that were developed in earlier studies [34-36] in conjunction with referencing of appropriate internal standards: PA 14:0/14:0, PC 14:0/14:0, PE 14:0/14:0, PG 15:0/15:0, PI 16:0/16:0, PS 14:0/14:0, BMP 14:0/14:0, APG 14:0/14:0, LPC 17:0, LPE 14:0, LPI 13:0, Cer d18:1/17:0, SM d18:1/12:0, dhSM d18:0/12:0, GalCer d18:1/12:0, GluCer d18:1/12:0, LacCer d18:1/12:0, D_7-cholesterol, CE 17:0, MG 17:0, 4ME 16:0 diether DG, D_5-TG 16:0/18:0/16:0 (Avanti Polar Lipids, Alabaster, AL).

Lipid Abbreviations

Free cholesterol, FC; cholesteryl ester, CE; monoacylglycerol, MG; diacylglycerol, DG; triacylglycerol, TG; ceramide, Cer; dihydroceramide, dhCer; sphingomyelin, SM; dihydrosphingomyelin, dhSM; galactosylceramide, GalCer; sulfatide, Sulf; glucosylceramide, GluCer; lactosylceramide, LacCer; monosialodihexosylganglioside, GM3; phosphatidic acid, PA; phosphatidylcholine, PC; ether phosphatidylcholine, PCe;

phosphatidylethanolamine, PE; plasmalogen phosphatidylethanolamine-, PEp; phosphatidylglycerol, PG; phosphatidylinositol, PI; phosphatidylserine, PS; lysophosphatidylcholine, LPC; ether lysophosphatidylcholine, LPCe; plasmalogen lysophosphatidylethanolamine, LPEp; lysophosphatidylinositol, LPI; bis(monoacylglycero)phosphate, BMP; Acyl phosphatidylglycerol, APG; NAPS; N-acyl phosphatidylserine, NAPS.

Statistical analysis of LC-MS

Lipid levels for each sample were calculated by summing up the total number of moles of all lipid species measured by LC-MS methodologies, and then normalizing individual lipid amounts to the total. The final data are presented as mean mol % with error bars showing mean ± S.E. For comparing the wild type and STARD4 knockdown U2OS-SRA cells, respectively, a two-tailed Student's T-test was used for statistical analysis. In all cases, *, $p < 0.05$; **, $p < 0.01$; ***, $p < 0.001$. For all bar graphs, error bars represent the mean ± S.E.

Immunostaining

Fixed cells were blocked and permeabilized for 15 min using 0.5% BSA by 0.05% (w/v) saponin in PBS. Cells were then stained overnight with ANTI-FLAG M2 antibody (F1804, lot number 124K61062, Sigma-Aldrich) at 1:1000 dilution at 4°C and AlecaFluor633 anti-mouse secondary antibody (Invitrogen) and 1:400 dilution for 30 min at room temperature.

Isolation of total RNA for RNA sequencing

Total RNA was isolated from wild type and STARD4 knockdown U2OS-SRA cells. The RNAeasy Plus Kit (Qiagen) that included a genomic DNA elimination step was used for RNA isolation. RNA concentration and purity were determined using Nanodrop (Thermo Scientific) and integrity was verified using Agilent 2100 Bioanalyzer (Agilent Technologies). Finally, all samples were used for library preparation and sequencing as 100 bp paired reads in 1.5 lanes of a HiSeq2500 following the protocols of Illumina Inc. (San Diego, CA) in the Genomics Resources Core Facility of Weill Cornell Medicine.

Transcriptome read alignment and data analysis

Quality control was performed using FastQC. STAR_2.4.0f1 was used for sequence alignment against the human genome build hg19, downloaded via the UCSC genome browser, and SAMTOOLS v0.1.19 for sorting and indexing reads. htseq-count v0.6.1 was used to get the counts of reads based on the UCSC RefGene GTF file for annotation (downloaded December 2015). Fragments per kilobase of transcript per million reads (FPKMs) for STARD4 knockdown and control U2OS cells were obtained using CuffLinks with default parameters. The log2 FPKM fold changes were calculated for paired samples, where positive fold change indicates up regulation in STARD4 knockdown samples, and where negative fold change represents down regulation.

Statistical analysis

All results are expressed as mean ± SE. The statistical significance of differences in mean values was determined by Student's *t*-test for pairwise comparison or ANOVA followed by Bonferroni correction for more than two groups.

RESULTS:

Cellular cholesterol levels increase following stable knockdown of STARD4.

To determine the contribution of STARD4 in intracellular sterol sensing and homeostasis, we utilized a U2OS cell line that stably expresses scavenger receptor A (SRA), U2OS-SRA [30]. These cells have been used previously to study sterol transport [10] and allow cholesterol loading through SRA-mediated uptake of modified lipoproteins. STARD4 protein levels were stably reduced using a pGFP-V-RS construct containing shRNA specific for STARD4. Following shRNA treatment, knockdown cells were selected using puromycin, and STARD4 levels in control U2OS-SRA and STARD4-KD cells were assessed by immunoblot. STARD4 protein levels were found to be reduced ~75% compared to control U2OS-SRA cells (Figure 1A-B). Notably, complete reduction of STARD4 in U2OS-SRA cells using CRISPR was lethal within 72 hours (unpublished observation), but STARD4-KD cells showed no change in growth rate compared to U2OS-SRA cells (Supplemental Figure 1.)We fixed and stained the cells with the cholesterol binding probe, filipin, to estimate cellular free cholesterol (FC) levels. Consistent with previous work [10, 11], stable reduction of STARD4 resulted in an increase in filipin intensity per cell, compared to U2OS-SRA cells, indicating a ~40% increase in the free cholesterol content (Figure 1C-D). We transiently transfected STARD4 KD cells with a shRNA-resistant mCherry-STARD4 construct 24 hours prior to fixation and staining with filipin, to exclude off-target activity of the shRNA that could impact filipin intensity independently of STARD4 levels. The co-expression of mCherry allowed us to distinguish between transiently transfected cells and STARD4-KD cells within individual fields. The increase in filipin intensity was reversed in mCherry-STARD4 expressing cells (Figure 1C-D), indicating the increased filipin intensity observed in the STARD4-KD cells was STARD4 specific.

The images in Figure 1 indicated that the STARD4-KD cells had bright filipin labeling outside of the ERC and plasma membrane, which we had identified previously as the main pools of cholesterol in U2OS-SRA cells. To examine this more closely, we used high resolution confocal imaging to look for filipin labeling of the ERC, which is labeled with endocytosed transferrin [37], and also filipin labeling of late endosomes containing endocytosed LDL [38]. As shown in Figure 2, there was filipin labeling of the ERC, and it appeared brighter in the STARD4-KD cells. However, when normalized to total cell fluorescence, there was no significant increase in the filipin labeling of the ERC. In the confocal images, we could see that there was a significant increase in the filipin labeling of LDL-containing late endosomes (Figure 2 A&C). This suggests that some unesterified cholesterol accumulates in late endosomes in STARD4-KD cells.

To make an estimate of changes in filipin labeling in the plasma membrane, we used the 20th percentile of the brightness in the epifluorescence image each cell as a measure of the filipin

brightness in broad areas of the plasma membrane (Figure 3A). We then multiplied this brightness by the area of the cell to estimate total plasma membrane labeling. (We also used the 40th percentile of brightness with similar results.) There is a small increase in filipin labeling of the plasma membrane (Figures 3 A&B). However, when this plasma membrane labeling is divided by total cell intensity, it shows a decrease (Figure 3C). This indicates that the largest percentage increase in filipin labeling is in punctate organelles in the cells.

Stable reduction of STARD4 reduces sterol transport.

Previous work has indicated that a large fraction of sterol transport is mediated by non-vesicular mechanisms [1, 6, 11]. As loss of STARD4 in cells results in altered cholesterol sensing [10, 11], and levels [10] (Figure 1), we investigated if stable reduction of STARD4 altered the kinetics of sterol transport between the plasma membrane and the ERC using fluorescence microscopy techniques [3, 10, 11]. We utilized fluorescence recovery after photobleaching (FRAP) to measure sterol transport to the ERC (Figure 4A). In U2OS-SRA cells, dehydroergosterol (DHE) was trafficked to the ERC with a halftime ($t_{1/2}$) of 12.4±1.0 min (Figure 4B). In STARD4-KD cells, we observed reduced sterol transport to the ERC with $t_{1/2}$ of 37.8±8.1 min (Figure 4 A-B). When STARD4-KD cells were rescued using mCherry-STARD4, sterol transport was restored, and cells exhibited a $t_{1/2}$ of 13.5±1.3 min. The data shown for the STARD4 knockdown cells fit well to a single first order rate process. These results are consistent with previous reports finding STARD4 as an important regulator of intracellular cholesterol transport [10, 11]. In order to get accurate rates, we made frequent measurements over a 10 minute period. This could not be extended due to photobleaching. To verify that the recovery is close to 100% at long times, we made infrequent measurements over 60 minutes. We obtained similar values for $t_{1/2}$, but now it can be seen that recovery goes to nearly 100% in both the U2OS-SRA and the STARD4-KD cells. The lines showing the fit to the data points are based on full recovery.

To determine whether STARD knockdown affected membrane transport of proteins, we measured the amount of fluorescent transferrin delivered to the ERC (Figure S2). This approach to steady state labeling of the ERC depends on the rates of endocytosis and intracellular sorting of membrane to the ERC as well as the rate of efflux from the ERC to the plasma membrane [37]. We found no difference in the rate of filling the ERC, indicating that these aspects of membrane trafficking are not affected by reduction of STARD4 levels.

Stable reduction of STARD4 increases detergent solubilization of the plasma membrane.

The increased cellular cholesterol levels (Figure 1) might be expected to increase the amount of ordered domains in cellular membranes. To investigate if the plasma membrane properties were altered following knockdown of STARD4, we examined the cold Triton X-100 (TX-100) solubilization of the plasma membrane using $DiIC_{16}$, which due to its long and saturated alkyl chains preferentially associates with detergent-resistant membranes [39-41] (Figure 5). This cold triton solubility assay has been used to document changes in bilayer properties associated with changes in cholesterol levels and acyl chain saturation [39, 42].

Prior to TX-100 extraction, both U2OS-SRA cells and STARD4-KD cells have uniform $DiIC_{16}$ plasma membrane labeling (Figure 5A). Consistent with previous work [39], the

plasma membrane of U2OS-SRA cells have holes in the $DiIC_{16}$ labeling after cold TX-100 extraction (Figure 5A), but a large fraction of the membrane remains labeled, indicating that a large fraction of the plasma membrane is detergent resistant. When STARD4 is stably knocked down, extraction of $DiIC_{16}$ is significantly increased (Figure 5B), indicating that more of the plasma membrane has been solubilized. To confirm this is a STARD4 specific effect, we transiently transfected the STARD4-KD cells with a shRNA resistant FLAG-STARD4 construct. The previously used shRNA resistant mCherry-STARD4 construct could not be used due to overlap in the emission spectra of mCherry and $DiIC_{16}$. We assessed the transfection rate to be ~80% by immunostaining using an anti-FLAG antibody (Figure S3). The reduced $DiIC_{16}$ intensity following TX-100 extraction was reversed when STARD4-KD cells were transiently transfected with FLAG-STARD4 (Figure 5A-B), confirming the effect to be STARD4-specific. These results suggest that the plasma membrane of STARD4-KD cells can be more easily solubilized and therefore is more disordered than in control U2OS-SRA cells. Thus, even with increased total cell cholesterol, the plasma membrane appears to be less ordered when STARD4 levels are reduced.

Stable reduction of STARD4 decreases plasma membrane order.

To validate that stable reduction of STARD4 in U2OS-SRA cells reduces membrane order, we utilized Laurdan, which has a lipid order dependent fluorescence emission shift and can be used to evaluate the plasma membrane order in living cells [43]. In more disordered membranes, Laurdan fluorescence emission is red shifted, while in ordered membranes, Laurdan florescence emission is blue shifted. The order-linked emission shift is typically expressed as a generalized polarization (GP) value, which can be calculated with the intensities at 440 nm and 470 nm according to the GP function, $GP = (I_{440} - I_{470})/(I_{440} + I_{470})$.

After a 30 minute incubation with Laurdan, the dye reaches equilibrium with the various cellular membranes [43]. The STARD4-KD cells stably express GFP, which is weakly fluorescent at 470 nm, so knockdown cells were imaged with or without Laurdan so that the background GFP signal could be corrected. Images were taken of Laurdan labeled cells at 440 nm and 470 nm and the GP calculated in regions of the plasma membrane. We observed that STARD4-KD cells displayed a lower GP value than control U2OS-SRA cells, as seen by a blue shift, indicating lower plasma membrane order (Figure 6A-B). This reduction in plasma membrane order could be restored by expression of shRNA-resistant mCherry-STARD4 (Figure 6A-B). Taken together, the cold TX-100 extraction (Figure 5) and Laurdan imaging (Figure 6) indicate that cells decrease their plasma membrane order following stable reduction of STARD4.

Reduction of STARD4 alters the lipidome profile.

The observations that STARD4 reduction led to decreased plasma membrane order even in the presence of increased cholesterol led us to analyze the lipidome of STARD4-KD and U2OS-SRA cells (Figure 7). The distribution of the individual molecular lipid species that were measured can be found in Supplemental Dataset S1.

Consistent with filipin labeling (Figure 1), STARD4 knockdown cells have an increase in FC compared to U2OS-SRA cells (Figure 7A). Interestingly, the concentration of 26 out of the 30 lipid classes identified by mass spectrometry showed a statistically significant difference between the U2OS-SRA and STARD4 knockdown cells (Figure 7A-G). Specifically, reduction of STARD4 resulted in increased FC, sphingomyelin (SM), dihydrosphingomyelin (dhSM), lactosylceramide (LacCer), plasmalogen phosphatidylethanolamine- (PEp), phosphatidylglycerol (PG), phosphatidylinositol (PI), phosphatidylserine (PS), plasmalogen lysophosphatidyl ethanolamine- (LPEp) and bis (monoacylglycero) phosphate (BMP). Additionally, several lipids had a lower abundance in STARD4 knockdown cells - most notably cholesterol ester (CE), monoacylglycerol (MG), diacylglycerol (DG), triacylglycerol (TG) ceramide (Cer) and phosphatidylcholine (PC). The abundance of several lipids was similar in STARD4 knockdown and U2OS-SRA cells, including galactosylceramide (GalCer), sulfatide (Sulf), glycosactosylceramide (GluCer) and phosphatidic acid (PA). Comparative lipidomic analysis of STARD4 knockdown U2OS-SRA and control U2OS-SRA cells indicates that stable reduction of STARD4 results in large alterations to the lipid composition of cellular membranes.

STARD4 knockdown increases phospholipid acyl chain length and unsaturation.

To further investigate the effects of STARD4 knockdown on the lipidome, we examined the acyl chain length (Figure 8A) and saturation level (Figure 8B) of glycerophospholipids and DG in U2OS-SRA and STARD4-KD cells. Analysis of the acyl chain length shows that stable reduction of STARD4 (red) results in a shift toward longer acyl chains compared to U2OS-SRA cells (blue). Specifically, U2OS-SRA cells are relatively enriched in short-medium (32-34C) chains, while STARD4 knockdown cells are relatively enriched in medium-long (36-42C) chains (Figure 8A). The increase in acyl chain lengths in STARD4 knockdown cells may contribute to disordered lipid packing leading to alterations in the membrane order [44].

Analysis of the acyl chain saturation of STARD4-KD (Figure 8B **red**) and U2OS-SRA (Figure 8B **blue**) cells also show alterations. The lipids from U2OS-SRA cells are relatively enriched in mono-, di- and tri-unsaturated fatty acids. In comparison, STARD4 knockdown cells are relatively enriched in polyunsaturated fatty acids with 4, 5 and 7 double bonds (Figure 8B). This increase in unsaturated fatty acids would likely alter the membrane order [1] and cold TX-100 solubility (Figure 5). Taken as a whole, the lipid profiling of STARD4 knockdown and U2OS-SRA cells shows that reduction of STARD4 results in alterations to the membrane composition (Figures 7 and 8).

Reduction of STARD4 alters RNA profile.

As stable reduction of STARD4 resulted in altered sterol levels (Figures 1 and 7), sterol transport (Figure 2) and membrane properties (Figure 5 & 6), we examined if reduction of STARD4 also altered RNA transcript levels. We investigated transcriptional changes by RNA-seq on matched STARD4-KD and U2OS-SRA samples and focused on genes known to be involved in cholesterol homeostasis or transport as well as genes involved in lipid saturation (Figure 9). The analysis of the all the genes that were annotated can be found in Supplemental Dataset S2.

Consistent with a previous study [10], reduction of STARD4 upregulates SREBP-2 processing and subsequently activates transcription of genes regulated by SREBP-2. HMG-CoA synthase 1 (HMGCS1) and HMG-CoA reductase (HMGCR) were upregulated in STARD4-KD cells compared to U2OS-SRA cells (Figure 9A). Interestingly, the LDL receptor (LDLR), which is a well-documented SREBP-2 target, was not upregulated. In addition to SREBP-2, the sterol responsive element-binding protein 1 (SREBP-1) was downregulated, while several fatty acid desaturases, including fatty acid desaturase 3 (FADS3), fatty acid desaturase 2 (FADS2) and sphingolipid delta(4)-desaturase DES1 (DEGS1) were notably upregulated in STARD4-KD samples (Figure 9B). Interestingly, the transcript levels of acyl-CoA desaturase (SCD) were not statistically altered between knockdown and control samples.

The transcript levels of some START domain proteins, SCP-2, and several members of the oxysterol-binding protein-related protein (OSBP) family of lipid transporters were downregulated (Figure 9C). Consistent with previous work [28], reduction of STARD4 resulted in a decrease in the transcript levels of Niemann Pick C1 (NPC1) protein. Notably, the transcript levels for STARD5 are upregulated significantly following stable reduction of STARD4. Taken as a whole our data show that stable reduction of STARD4 in U2OS-SRA cells results in large alterations in expression of genes involved in lipid metabolism and transport.

DISCUSSION:

Although a large fraction of cholesterol transport is mediated by non-vesicular transport mechanisms, the role of specific sterol transfer proteins in maintaining cholesterol homeostasis remains poorly understood. STARD4, a soluble sterol transporter, has been implicated in maintaining sterol homeostasis and is transcriptionally regulated by SREBP-2 [10, 11, 27, 45]. In this study, we studied the effects of stable STARD4 knockdown to investigate the role of STARD4 in cholesterol sensing and lipid homeostasis. We show that stable reduction of STARD4 causes an increase in cellular cholesterol level and slowed sterol transport between the ERC and the plasma membrane. Additionally, reduction of STARD4 results in reduced plasma membrane order, alterations to the cellular lipidome and transcription profile. Thus, STARD4 is a critical component in the regulatory machinery that senses and maintains sterol levels and lipid homeostasis.

It has been challenging to demonstrate that a specific sterol transfer protein plays a major role in maintaining cholesterol distribution and homeostasis [1, 2]. One of the difficulties in this endeavor is that there are several sterol binding proteins that could transport cholesterol between organelles, and many of these proteins may have overlapping functions [6, 46]. Additionally, there is evidence that knockout of lipid transporters may result in selective up regulation of other lipid transporters as a compensatory mechanism. This is most evident in cells that have been knocked out for SCP-2/SCP-X where loss of these proteins induces an up regulation of STARD4 and PCTP/STARD2 [47]. In mammalian cells, STARD4 has been implicated as an important sterol transporter [1, 10, 11, 27], but the development and survival of a *StarD4*$^{-/-}$ mouse indicates that the gene is not essential [28]. While reduction of STARD4 in either cell culture models [10, 11] or mice [28] resulted in some alterations, it

is possible that loss of STARD4 results in activation of compensatory mechanisms, which can vary among tissues [48], to ensure viability [47]. It is paradoxical that complete loss of STARD4 in U2OS-SRA cells is lethal after a few days, but a homozygous *Stard4*$^{-/-}$ mouse can live and breed [28]. We do not understand the reason for this other than to guess that adaptations early in development allow the knockout mice to survive. A more complete analysis of lipidomics and gene expression in the knockout mice may be informative.

Analysis of the RNA profiles of STARD4 knockdown and U2OS-SRA cells showed that the reduction in sterol transport rate was unlikely to be mediated exclusively by altered expression of other soluble sterol transport proteins. There were increases in RNA expression of some sterol transport proteins, most notably STARD5 (Figure 9C). We note that ~25-30% of the endogenous STARD4 protein remains in STARD4-KD cells. Other sterol transport proteins including members of the START, ORP/OSBP family as well as SCP-2 had decreased RNA transcript levels following stable reduction of STARD4.

We further investigated the link between changes in sterol transport and lipid alterations by examining the genes involved in lipid homeostasis and the cellular lipidome (Figure 7 & 8). Cholesterol levels in the ER are maintained in a narrow range [5]. These levels are determined by a balance between sterol synthesis and delivery to the ER, which increase sterol levels, and sterol efflux or esterification, which decrease sterol in the ER. As STARD4 delivers sterol to the ER [1, 10, 11, 17], reduction of STARD4 would reduce delivery of cholesterol to the ER, altering cellular cholesterol homeostasis. Therefore, it was not surprising that stable reduction of STARD4 caused an upregulation of SREBP-2 [10] and genes involved in cholesterol biosynthesis and uptake. Consistent with this, cholesterol levels were increased in STARD4 knockdown cells. It is also worth noting that both the alpha and beta isoforms of the liver x-receptor, NR1H3 and NR1H2 respectively, had reduced transcript levels in the STARD4 knockdown cells. This suggests that multiple pathways maintaining cholesterol homeostasis are altered when STARD4 levels are reduced.

One of the most important changes may be the reduction in *NPC1* and *NPC2* mRNA expression. NPC1 and NPC2 are required for efflux of cholesterol out of late endosomes and lysosomes, and we observed that there was a large increase in the unesterified cholesterol in these organelles in STARD4-KD cells. Thus, even though there was some increase in the filipin labeling of the plasma membrane, the increase in total cell cholesterol was greater than the plasma membrane increase due to the increased cholesterol in intracellular organelles.

In addition to changes in cholesterol metabolism, there were global changes in the lipidome of the STARD4-KD cells. Several other lipids, including sphingomyelin and phosphatidylserine, were highly enriched in STARD4-KD cells. This increase in sphingomyelin is somewhat surprising as it is known to be enriched on the exofacial leaflet of the plasma membrane [49] and associated with high lipid order [50], but the plasma membrane of STARD4-KD cells were more sensitive to cold TX-100 extraction and had reduced general polarization indicating a more disordered membrane. It is likely that the increase in lipid unsaturation is responsible for the decreased overall lipid order in the plasma membrane. It is possible that the increase in acyl chain length is also related to the

increase in unsaturation since polyunsaturated acyl chains tend to be longer than saturated lipids.

Further research will be required to understand how reduced STARD4 levels lead to transcriptional changes that are associated with these changes in lipid profiles. In addition to altering SREBP-2 transcription levels and regulation, stable reduction of STARD4 also resulted in lower transcript levels for SREBP-1. Interestingly, we found that some lipid desaturases were upregulated following STARD4 knockdown. The increased expression of these desaturases could account, in part, for the increase in polyunsaturation of lipid acyl chains. The rise in unsaturated lipids would decrease membrane order [51], and further studies will be required to understand how primary changes in cholesterol transport lead to such pleiotropic effects on lipid metabolism. One possibility is that changes in cholesterol levels lead to changes in lipid-lipid interactions and bilayer properties, which in turn lead to further homeostatic adaptations.

In summary, the stable reduction of STARD4 results in increased cellular cholesterol levels and slower sterol transport between the plasma membrane and the ERC in STARD4-KD cells compared to control U2OS-SRA cells. In addition to these effects, we observed alterations to the transcriptional and lipidomic profiles, which alters the biophysical properties of cell membranes. Reduction of STARD4 not only alters the regulation of the cholesterol homeostatic machinery but also modulates pathways involved in maintaining lipid homeostasis. Therefore, STARD4 expression must be finely tuned. Our data shows that dysregulation of STARD4 expression results in desensitization of the ER homeostatic machinery and changes to the lipidome and transcriptome of the cell. Thus, we propose that STARD4 is a critical component in the regulatory machinery that senses and maintains sterol levels and participates in maintaining lipid homeostasis.

Supplementary Material

Refer to Web version on PubMed Central for supplementary material.

ACKNOWLEDGEMENTS:

We would like to thank Genomics Resources Core Facility of Weill Cornell Medicine for technical assistance. We would also like to thank Dr. Mingming Hao (Weill Cornell) for critical reading and discussion of the manuscript.

FUNDING: This work was supported by National Institutes of Health grants F31-DK104631 (DBI), R01-CA194547 (OE), R01-NS056049 (GDP) and R01-GM123462 (FRM). The content is solely the responsibility of the authors and does not necessarily represent the official views of the National Institutes of Health. R.K.S. is an American Heart Association Stanley Stahl Postdoctoral Fellow (ID: 15POST22990022).

Abbreviations:

DHE	Dehydroergosterol
ER	endoplasmic reticulum
ERC	endocytic recycling compartment
FRAP	fluorescence recovery after photobleaching

MCD	Methyl-β-cyclodextrin
SCAP	SREBP-cleavage-activating protein
SRA	scavenger receptor A
SREBP-1	sterol responsive element-binding protein 1
SREBP-2	sterol responsive element-binding protein 2
StAR	steroidogenic acute regulatory protein
START	StAR-related lipid-transfer
Tf	transferrin
POPC	1-palmitoyl-2-oleoyl-sn-glycero-3-phosphatidylcholine
POPE	1-palmitoyl-2-oleoyl-sn-glycero-3-phosphatidylethanolamine
POPS	1-palmitoyl-2-oleoyl-sn-glycero-3-phosphatidylserine
PI	phosphatidylinositol
dansyl-PE	dansyl-phosphatidylethanolamine
TX	Triton X

REFERENCES

[1]. Iaea DB, Maxfield FR, Cholesterol trafficking and distribution, Essays Biochem, 57 (2015) 43–55. [PubMed: 25658343]

[2]. Mesmin B, Maxfield FR, Intracellular sterol dynamics, Biochim Biophys Acta, 1791 (2009) 636–645. [PubMed: 19286471]

[3]. Hao M, Lin SX, Karylowski OJ, Wustner D, McGraw TE, Maxfield FR, Vesicular and non-vesicular sterol transport in living cells. The endocytic recycling compartment is a major sterol storage organelle, J Biol Chem, 277 (2002) 609–617. [PubMed: 11682487]

[4]. Ikonen E, Cellular cholesterol trafficking and compartmentalization, Nat Rev Mol Cell Biol, 9 (2008) 125–138. [PubMed: 18216769]

[5]. Radhakrishnan A, Goldstein JL, McDonald JG, Brown MS, Switch-like control of SREBP-2 transport triggered by small changes in ER cholesterol: a delicate balance, Cell Metab, 8 (2008) 512–521. [PubMed: 19041766]

[6]. Maxfield FR, Menon AK, Intracellular sterol transport and distribution, Curr Opin Cell Biol, 18 (2006) 379–385. [PubMed: 16806879]

[7]. Blanchette-Mackie EJ, Pentchev PG, Cholesterol distribution in Golgi, lysosomes, and endoplasmic reticulum., In Intracellular Cholesterol Trafficking, (1998) 53–74.

[8]. Mobius W, van Donselaar E, Ohno-Iwashita Y, Shimada Y, Heijnen HFG, Slot JW, Geuze HJ, Recycling compartments and the internal vesicles of multivesicular bodies harbor most of the cholesterol found in the endocytic pathway, Traffic, 4 (2003) 222–231. [PubMed: 12694561]

[9]. Liscum L, Munn NJ, Intracellular cholesterol transport, Biochim Biophys Acta, 1438 (1999) 19–37. [PubMed: 10216277]

[10]. Mesmin B, Pipalia NH, Lund FW, Ramlall TF, Sokolov A, Eliezer D, Maxfield FR, STARD4 abundance regulates sterol transport and sensing, Molecular Biology of the Cell, 22 (2011) 4004–4015. [PubMed: 21900492]

[11]. Garbarino J, Pan M, Chin HF, Lund FW, Maxfield FR, Breslow JL, STARD4 knockdown in HepG2 cells disrupts cholesterol trafficking associated with the plasma membrane, ER, and ERC, J Lipid Res, 53 (2012) 2716–2725. [PubMed: 23033213]

[12]. Maxfield FR, Wustner D, Intracellular cholesterol transport, J Clin Invest, 110 (2002) 891–898. [PubMed: 12370264]

[13]. Iaea DB, Gale SE, Bielska AA, Krishnan K, Fujiwara H, Jiang H, Maxfield FR, Schlesinger PH, Covey DF, Schaffer JE, Ory DS, A novel intrinsically fluorescent probe for study of uptake and trafficking of 25-hydroxycholesterol, Journal of Lipid Research, 56 (2015) 2408–2419. [PubMed: 26497473]

[14]. Lange Y, Steck TL, Cholesterol homeostasis and the escape tendency (activity) of plasma membrane cholesterol, Prog Lipid Res, 47 (2008) 319–332. [PubMed: 18423408]

[15]. Brown MS, Goldstein JL, The SREBP pathway: regulation of cholesterol metabolism by proteolysis of a membrane-bound transcription factor, Cell, 89 (1997) 331–340. [PubMed: 9150132]

[16]. Liscum L, Faust JR, The intracellular transport of low density lipoprotein-derived cholesterol is inhibited in Chinese hamster ovary cells cultured with 3-beta-[2-(diethylamino)ethoxy]androst-5-en-17-one, J Biol Chem, 264 (1989) 11796–11806. [PubMed: 2745416]

[17]. Iaea DB, Dikiy I, Kiburu I, Eliezer D, Maxfield FR, STARD4 Membrane Interactions and Sterol Binding, Biochemistry, 54 (2015) 4623–4636. [PubMed: 26168008]

[18]. Beh CT, McMaster CR, Kozminski KG, Menon AK, A detour for yeast oxysterol binding proteins, J Biol Chem, 287 (2012) 11481–11488. [PubMed: 22334669]

[19]. Soccio RE, Breslow JL, StAR-related lipid transfer (START) proteins: mediators of intracellular lipid metabolism, J Biol Chem, 278 (2003) 22183–22186. [PubMed: 12724317]

[20]. Gatta AT, Wong LH, Sere YY, Calderon-Norena DM, Cockcroft S, Menon AK, Levine TP, A new family of StART domain proteins at membrane contact sites has a role in ER-PM sterol transport, Elife, 4 (2015).

[21]. Gallegos AM, Atshaves BP, Storey SM, McIntosh AL, Petrescu AD, Schroeder F, Sterol carrier protein-2 expression alters plasma membrane lipid distribution and cholesterol dynamics, Biochemistry, 40 (2001) 6493–6506. [PubMed: 11371213]

[22]. Puglielli L, Rigotti A, Greco AV, Santos MJ, Nervi F, Sterol carrier protein-2 is involved in cholesterol transfer from the endoplasmic reticulum to the plasma membrane in human fibroblasts, J Biol Chem, 270 (1995) 18723–18726. [PubMed: 7642518]

[23]. Clark BJ, The mammalian START domain protein family in lipid transport in health and disease, J Endocrinol, 212 (2012) 257–275. [PubMed: 21965545]

[24]. Alpy F, Tomasetto C, Give lipids a START: the StAR-related lipid transfer (START) domain in mammals, J Cell Sci, 118 (2005) 2791–2801. [PubMed: 15976441]

[25]. Iaea DB, Mao S, Maxfield FR, Steroidogenic Acute Regulatory Protein-related Lipid Transfer (START) Proteins in Non-vesicular Cholesterol Transport, in: Clark BJ, Stocco DM (Eds.) Cholesterol Transporters of the START Domain Protein Family in Health and Disease, Springer New York, 2014, pp. 173–188.

[26]. Rodriguez-Agudo D, Calderon-Dominguez M, Ren S, Marques D, Redford K, Medina-Torres MA, Hylemon P, Gil G, Pandak WM, Subcellular localization and regulation of StarD4 protein in macrophages and fibroblasts, Biochim Biophys Acta, 1811 (2011) 597–606. [PubMed: 21767660]

[27]. Soccio RE, Adams RM, Romanowski MJ, Sehayek E, Burley SK, Breslow JL, The cholesterol-regulated StarD4 gene encodes a StAR-related lipid transfer protein with two closely related homologues, StarD5 and StarD6, Proc Natl Acad Sci U S A, 99 (2002) 6943–6948. [PubMed: 12011452]

[28]. Riegelhaupt JJ, Waase MP, Garbarino J, Cruz DE, Breslow JL, Targeted disruption of steroidogenic acute regulatory protein D4 leads to modest weight reduction and minor alterations in lipid metabolism, J Lipid Res, 51 (2010) 1134–1143. [PubMed: 19965609]

[29]. Buton X, Mamdouh Z, Ghosh R, Du H, Kuriakose G, Beatini N, Grabowski GA, Maxfield FR, Tabas I, Unique cellular events occurring during the initial interaction of macrophages with matrix-retained or methylated aggregated low density lipoprotein (LDL). Prolonged cell-surface

contact during which ldl-cholesteryl ester hydrolysis exceeds ldl protein degradation, J Biol Chem, 274 (1999) 32112–32121. [PubMed: 10542246]

[30]. Majumdar A, Capetillo-Zarate E, Cruz D, Gouras GK, Maxfield FR, Degradation of Alzheimer's amyloid fibrils by microglia requires delivery of ClC-7 to lysosomes, Mol Biol Cell, 22 (2011) 1664–1676. [PubMed: 21441306]

[31]. Sheets ED, Holowka D, Baird B, Critical role for cholesterol in Lyn-mediated tyrosine phosphorylation of FcepsilonRI and their association with detergent-resistant membranes, J Cell Biol, 145 (1999) 877–887. [PubMed: 10330413]

[32]. Pipalia NH, Hao M, Mukherjee S, Maxfield FR, Sterol, protein and lipid trafficking in Chinese hamster ovary cells with Niemann-Pick type C1 defect, Traffic, 8 (2007) 130–141. [PubMed: 17156101]

[33]. Pipalia NH, Huang A, Ralph H, Rujoi M, Maxfield FR, Automated microscopy screening for compounds that partially revert cholesterol accumulation in Niemann-Pick C cells, J Lipid Res, 47 (2006) 284–301. [PubMed: 16288097]

[34]. Chan RB, Oliveira TG, Cortes EP, Honig LS, Duff KE, Small SA, Wenk MR, Shui G, Di Paolo G, Comparative lipidomic analysis of mouse and human brain with Alzheimer disease, J Biol Chem, 287 (2012) 2678–2688. [PubMed: 22134919]

[35]. Hsu FF, Turk J, Shi Y, Groisman EA, Characterization of acylphosphatidylglycerols from Salmonella typhimurium by tandem mass spectrometry with electrospray ionization, J Am Soc Mass Spectrom, 15 (2004) 1–11. [PubMed: 14698549]

[36]. Guan Z, Li S, Smith DC, Shaw WA, Raetz CR, Identification of N-acylphosphatidylserine molecules in eukaryotic cells, Biochemistry, 46 (2007) 14500–14513. [PubMed: 18031065]

[37]. Maxfield FR, McGraw TE, Endocytic recycling, Nat Rev Mol Cell Biol, 5 (2004) 121–132. [PubMed: 15040445]

[38]. Pipalia NH, Subramanian K, Mao S, Ralph H, Hutt DM, Scott SM, Balch WE, Maxfield FR, Histone deacetylase inhibitors correct the cholesterol storage defect in most Niemann-Pick C1 mutant cells, J Lipid Res, 58 (2017) 695–708. [PubMed: 28193631]

[39]. Hao M, Mukherjee S, Maxfield FR, Cholesterol depletion induces large scale domain segregation in living cell membranes, Proc Natl Acad Sci U S A, 98 (2001) 13072–13077. [PubMed: 11698680]

[40]. Mukherjee S, Zha X, Tabas I, Maxfield FR, Cholesterol distribution in living cells: fluorescence imaging using dehydroergosterol as a fluorescent cholesterol analog, Biophys J, 75 (1998) 1915–1925. [PubMed: 9746532]

[41]. Schroeder F, Barenholz Y, Gratton E, Thompson TE, A fluorescence study of dehydroergosterol in phosphatidylcholine bilayer vesicles, Biochemistry, 26 (1987) 2441–2448. [PubMed: 3607026]

[42]. Sun Y, Hao M, Luo Y, Liang CP, Silver DL, Cheng C, Maxfield FR, Tall AR, Stearoyl-CoA desaturase inhibits ATP-binding cassette transporter A1-mediated cholesterol efflux and modulates membrane domain structure, J Biol Chem, 278 (2003) 5813–5820. [PubMed: 12482877]

[43]. Owen DM, Rentero C, Magenau A, Abu-Siniyeh A, Gaus K, Quantitative imaging of membrane lipid order in cells and organisms, Nat Protoc, 7 (2011) 24–35. [PubMed: 22157973]

[44]. McConnell HM, Radhakrishnan A, Condensed complexes of cholesterol and phospholipids, Biochim Biophys Acta, 1610 (2003) 159–173. [PubMed: 12648771]

[45]. Soccio RE, Adams RM, Maxwell KN, Breslow JL, Differential gene regulation of StarD4 and StarD5 cholesterol transfer proteins. Activation of StarD4 by sterol regulatory element-binding protein-2 and StarD5 by endoplasmic reticulum stress, J Biol Chem, 280 (2005) 19410–19418. [PubMed: 15760897]

[46]. Raychaudhuri S, Prinz WA, The diverse functions of oxysterol-binding proteins, Annu Rev Cell Dev Biol, 26 (2010) 157–177. [PubMed: 19575662]

[47]. Storey SM, McIntosh AL, Huang H, Landrock KK, Martin GG, Landrock D, Payne HR, Atshaves BP, Kier AB, Schroeder F, Intracellular cholesterol-binding proteins enhance HDL-mediated cholesterol uptake in cultured primary mouse hepatocytes, Am J Physiol Gastrointest Liver Physiol, 302 (2012) G824–839. [PubMed: 22241858]

[48]. Unger RH, Clark GO, Scherer PE, Orci L, Lipid homeostasis, lipotoxicity and the metabolic syndrome, Biochim Biophys Acta, 1801 (2010) 209–214. [PubMed: 19948243]

[49]. Testi R, Sphingomyelin breakdown and cell fate, Trends Biochem Sci, 21 (1996) 468–471. [PubMed: 9009829]

[50]. Huang J, Feigenson GW, A microscopic interaction model of maximum solubility of cholesterol in lipid bilayers, Biophys J, 76 (1999) 2142–2157. [PubMed: 10096908]

[51]. Xu X, London E, The effect of sterol structure on membrane lipid domains reveals how cholesterol can induce lipid domain formation, Biochemistry, 39 (2000) 843–849. [PubMed: 10653627]

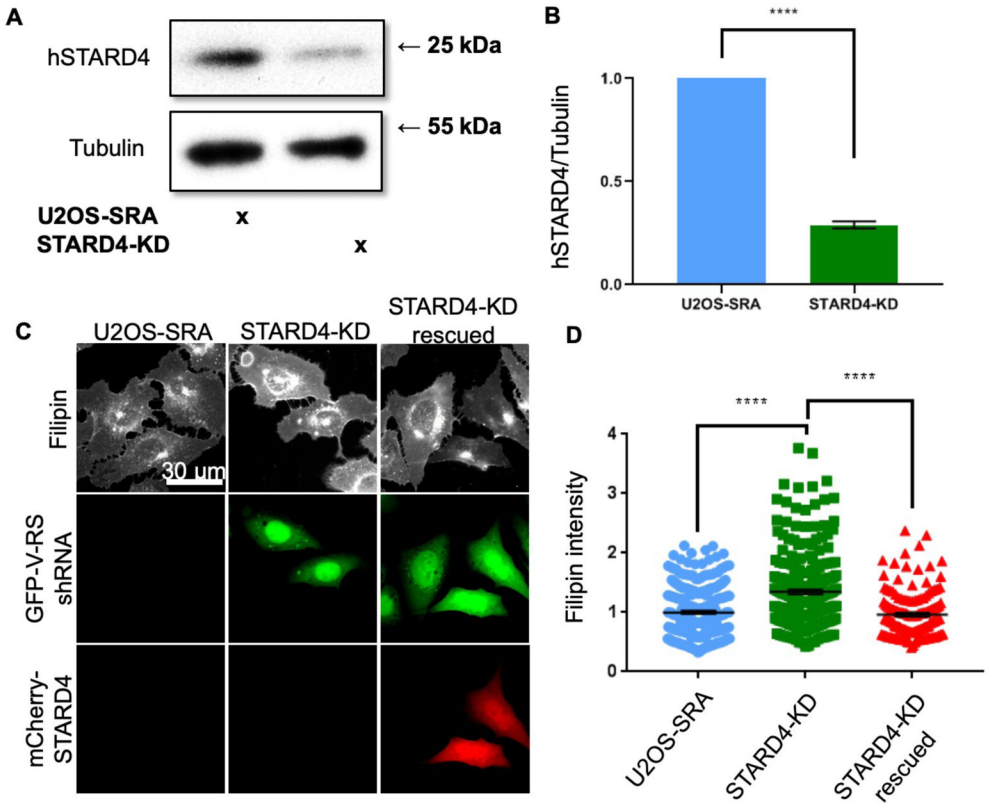

Figure 1. Stable knockdown of STARD4 increases filipin staining and can be reversed by transient expression of shRNA-resistant mCherry-STARD4.

(A) U2OS-SRA cells were transfected with pGFP-V-RS shRNA expressing a shRNA sequence against STARD4. Generation of stable STARD4 knockdown in U2OS-SRA cells (STARD4-KD) was achieved by selection with 5 μg/mL puromycin. The immunoblot shows the efficiency of STARD4 silencing. (B) STARD4 protein levels relative to tubulin levels in U2OS-SRA and STARD4-KD cells were quantified from 3 independent immunoblot experiments. (C) Epifluorescence microscopy images of U2OS-SRA, STARD4-KD, or STARD4-KD cells transfected with shRNA-resistant mCherry-STARD4 construct to rescue STARD4 expression (STARD4-KD rescued), which were fixed and stained with filipin. (D) Microscopy images were used to quantify cellular filipin fluorescence from >200 cells per group. **** $p < 0.0001$. Error bars sem.

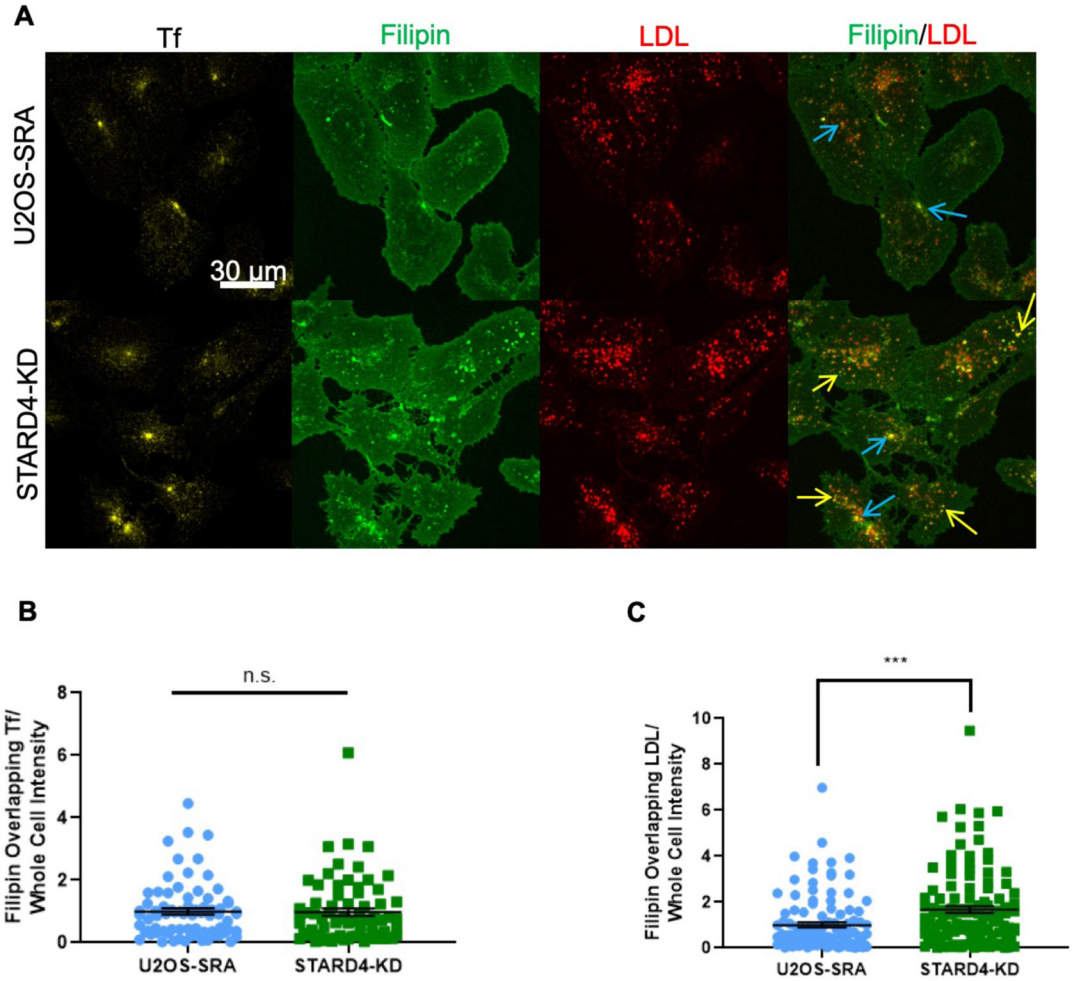

Figure 2. STARD4-KD cells show cholesterol accumulation in endosomes.

U2OS-SRA and STARD4-KD cells were incubated with LDL-A633 (10 μg/mL) for 1 hour prior to fixation and with Tf-A546 (20 μg/ml) 25 minutes prior to fixation. Fixed U2OS-SRA and STARD4-KD cells were stained with filipin (50 μg/ml) for 45 minutes and imaged immediately after by confocal microscopy. (A) Maximum projections of confocal stacks illustrate the differences in filipin stain with colocalization of filipin puncta and LDL-A633. Yellow arrows indicate areas of overlap between filipin and LDL. Blue arrows indicate areas of overlap between filipin and transferrin. (B) Tf-A546 stained ERC showed no difference in filipin distribution in >70 cells per group. Error bars, sem. (C) LDL-containing intracellular compartments showed an increased filipin distribution in >100 cells per group *** $p < 0.001$. Error bars sem.

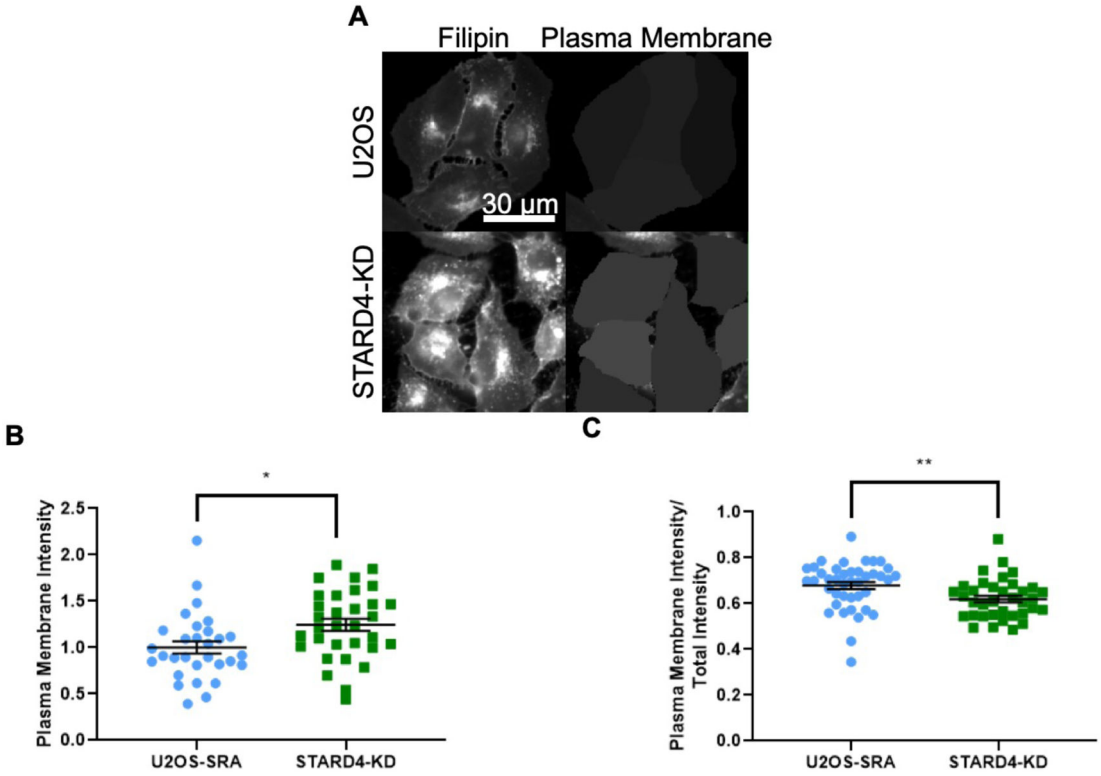

Figure 3. STARD4-KD total plasma membrane intensity increases.

(A) Epifluorescence microscopy images of U2OS-SRA or STARD4 KD cells fixed and stained with filipin. The right panels show the whole cells filled with the brightness of the 20th percentile pixel in each cell. (B) Calculated plasma membrane intensity of STARD4-KD cells is larger than U2OS-SRA cells measured in >30 cells per group * $p < 0.05$. Error bars, sem. (C) The increase in STARD4-KD plasma membrane cholesterol is less than the increase in the whole cells in >30 cells per group ** $p < 0.01$. Error bars, sem.

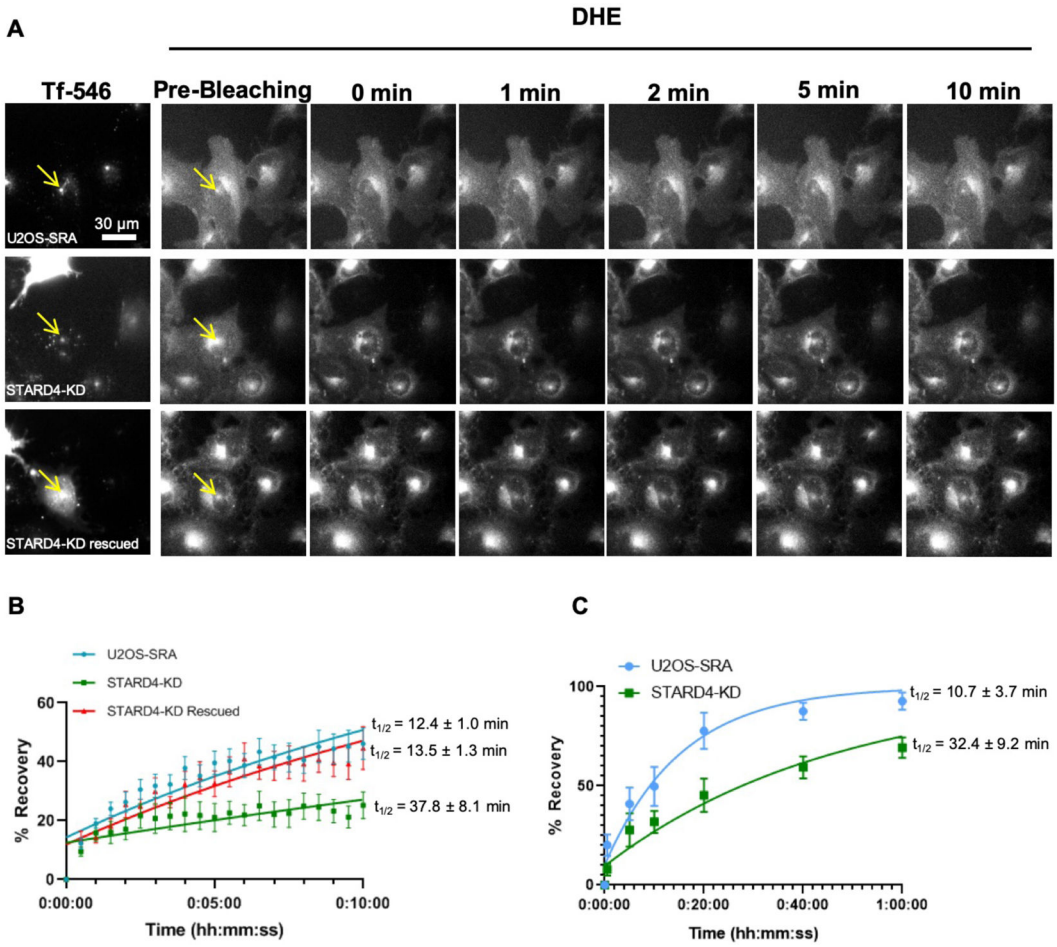

Figure 4. Sterol transport to the ERC is reduced following stable knockdown of STARD4.

For FRAP experiments, control U2OS-SRA cells , STARD4 knockdown, and STARD4-KD cells transfected with shRNA-resistant mCherry-STARD4 were labeled with DHE for 120 minutes. In the last 20 minutes, cells were incubated with 20 µg/ml transferrin-Alexa-546 at 37°C to identify the ERC. Cells were maintained at 37°C. (A) Images of transferrin-Alexa-546 and DHE were taken before photobleaching. DHE in the ERC was photo-bleached (yellow arrow), and images were taken every 30 seconds. (B) Fluorescence images were used to quantify FRAP for U2OS-SRA, STARD4-KD and STARD4-KD rescued cells. Each data point is derived from an average of at least 13 cells. Error bars sem. Data are fit to single exponential that approaches one hundred percent recovery. (C) Extended FRAP experiments. Each data point is derived from an average of at least 4 cells. Error bars, sem.

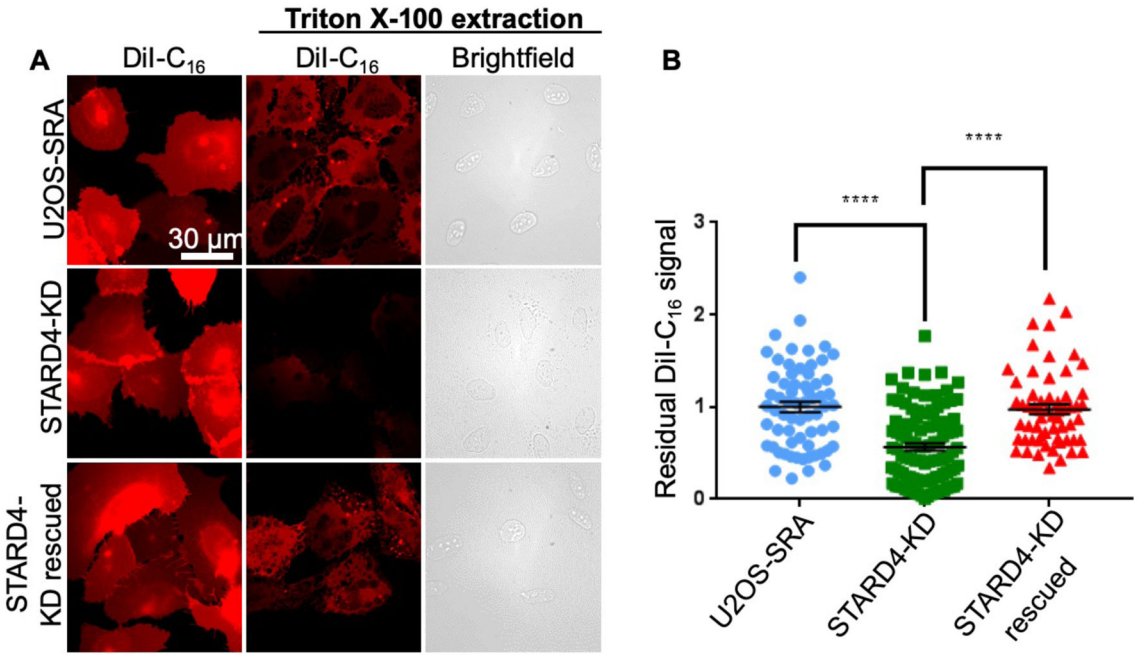

Figure 5. Stable knockdown of STARD4 increases plasma membrane solubilization by cold TX-100 and can be reversed by transient expression of shRNA-resistant FLAG-STARD4.

(A) Epifluorescence microscopy images of U2OS-SRA, STARD4-KD and STARD4-KD rescued cells (transiently transfected with shRNA resistant pCMV-Tag2b-STARD4 plasmid). Cells were incubated with DiI-C_{16} alone or incubated with DiI-C_{16} and then extracted using TX-100 prior to imaging. Brightfield images are also shown for cells after TX-100 extraction. (B) Microscopy images were used to quantify residual DiI-C_{16} fluorescence after TX-100 extraction from >200 cells per group. **** $p < 0.0001$. Error bars sem.

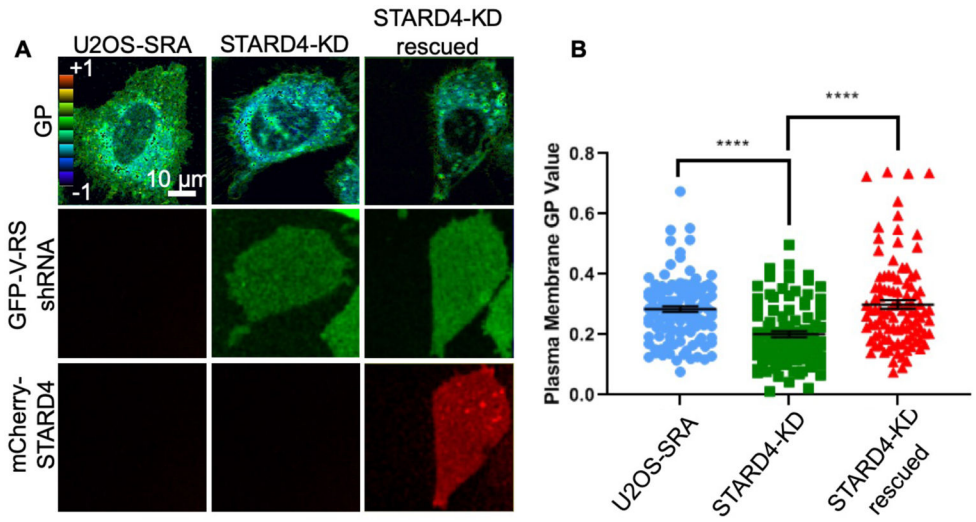

Figure 6. Stable knockdown of STARD4 increases plasma membrane fluidity and can be reversed by transient expression of shRNA-resistant mCherry-STARD4.

(A) Epifluorescence microscopy images of U2OS-SRA, STARD4-KD and STARD4-KD rescued cells (transiently transfected with shRNA resistant mCherry-STARD4 construct). Cells were incubated with Laurdan at a final concentration of 25μM for 30 minutes, and images obtained, from which generalized polarization (GP) images were generated. (B) Microscopy images were used to quantify GP (normalized to control) at the plasma membrane from >100 cells per group. **** $p < 0.0001$. Error bars sem.

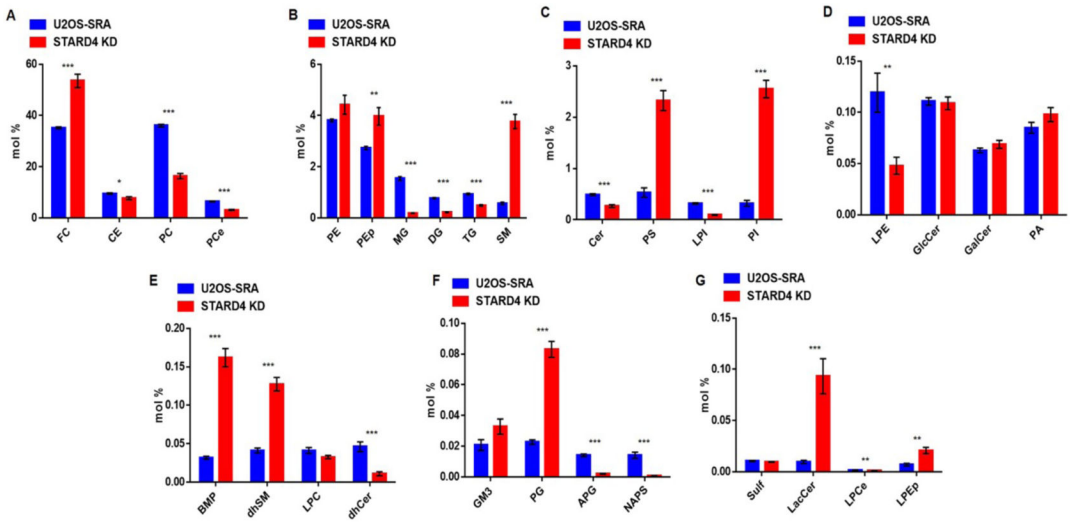

Figure 7: Alteration in lipid composition of U2OS-SRA following stable knockdown of STARD4.

Lipid profile of wild type (blue) and STARD4 knockdown (red) U2OS-SRA cells. (A) Free cholesterol, cholesterol ester, phosphatidylcholine, and ether phosphatidylcholine. (B) Phosphatidylethanolamine, phosphatidylethanolamine-plasmalogen, monoacylglycerol, diacylglycerol, triacylglycerol, and sphingomyelin. (C) Ceramide, phosphatidylserine, lysophosphatidylinositol, and phosphatidylinositol. (D) Lysophosphatidyl ethanolamine, glucosylceramide, galactosylceramide and phosphatidic acid. (E) bis(monoacylglycero)phosphate, dihydrosphingomyelin, lysophosphatidylcholine, and dihydroceramide. (F) Monosialodihexosylganglioside, phosphatidylglycerol, acyl phosphatidylglycerol and N-acyl phosphatidylserine. (G) Sulfatide, lactosylceramide, ether lysophosphatidylcholine and plasmalogen lysophosphatidylethanolamine. Lipid subclasses are expressed as mol % of total lipids measured from 6 samples per condition. Error bars sem. * $p < 0.05$; **, $p < 0.01$; ***, $p < 0.001$. The absolute level of individual lipid species is presented in supplemental Dataset S1.

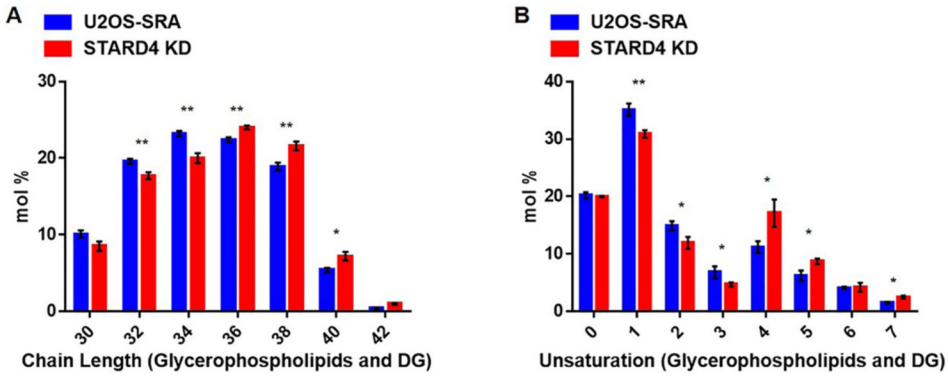

Figure 8: Acyl chain length and unsaturation level increase in STARD4 knockdown U2OS-SRA cells.

Acyl chain length and saturation profile of wild type (blue) and STARD4 knockdown (red) U2OS-SRA cells. (A) Chain length and (B) saturation level of glycerophospholipids and diacylglycerol in wild type and STARD4 knockdown U2OS-SRA cells. Glycerophospholipid and diacylglycerol chain length is the sum of the lipid acyl chains. Glycerophospholipid and diacylglycerol chain length and saturation level are expressed as mean mol % of total phospholipids and diacylglycerol measured from 6 samples per condition. Error bars sem. * $p < 0.05$; **, $p < 0.01$.

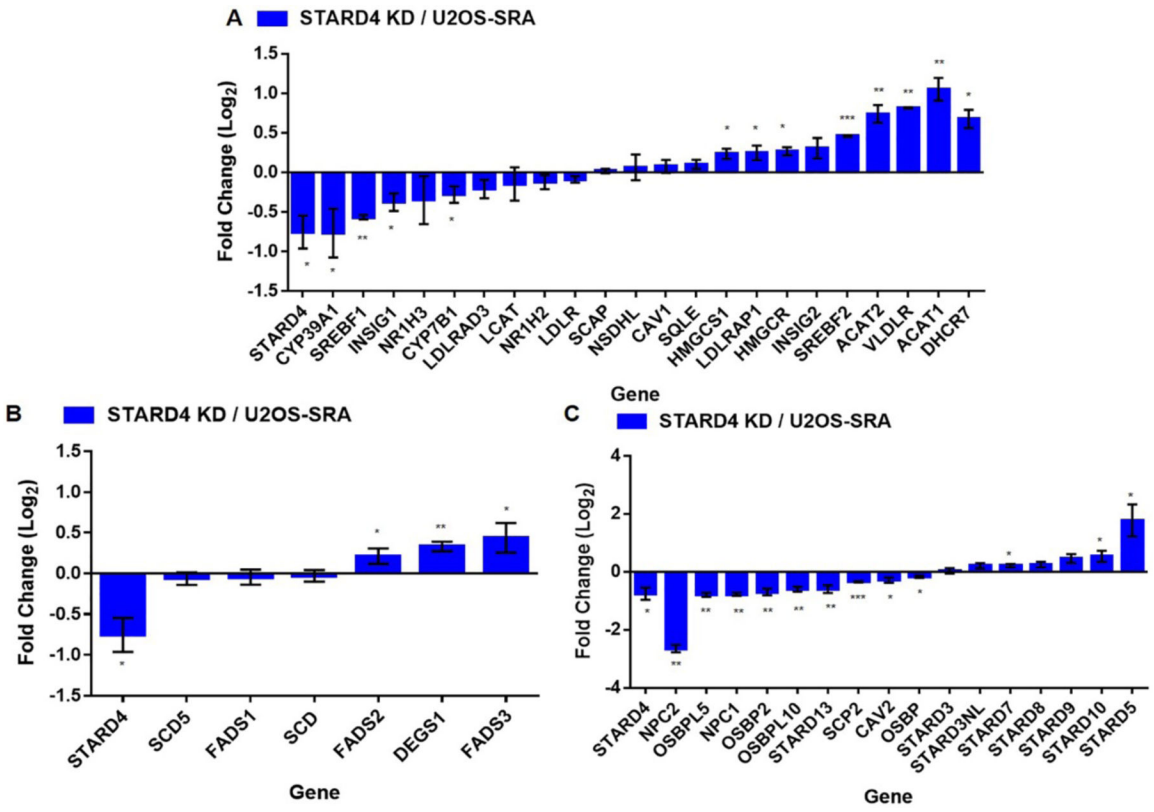

Figure 9: Altered RNA profile of stable STARD4 knockdown U2OS-SRA cells.

Differential gene expression of (A) cholesterol homeostatic machinery, (B) fatty acid desaturases and (C) sterol transporters in wild type and STARD4 knockdown U2OS-SRA cells. As a standard, STARD4 gene expression is included in each group. Average log2 fold changes of genes. 3 samples were analyzed per condition. Error bars sem. * $p < 0.05$; **, $p < 0.01$; ***, $p < 0.001$. The absolute level of individual genes is presented in supplemental Dataset S2.